S^5Mars: Semi-Supervised Learning for Mars Semantic Segmentation

Jiahang Zhang, Lilang Lin, *Student Member, IEEE*, Zejia Fan,
Wenjing Wang, *Graduate Student Member, IEEE*, and Jiaying Liu, *Senior Member, IEEE*

***Abstract*— Deep learning has become a powerful tool for Mars exploration. Mars terrain semantic segmentation is an important Martian vision task, which is the base of rover autonomous planning and safe driving. However, there is a lack of sufficient detailed and high-confidence data annotations that are exactly required by most deep learning methods to obtain a good model. To address this problem, we propose our solution from the perspective of joint data and method design. We first present a new dataset S^5Mars for semi-supervised learning on Mars semantic segmentation, which contains 6k high-resolution images and is sparsely annotated based on confidence, ensuring the high quality of labels. Then, to learn from this sparse data, we propose a semi-supervised learning (SSL) framework for Mars image semantic segmentation to learn representations from limited labeled data. Different from the existing SSL methods that are mostly targeted at the Earth image data, our method takes into account Mars data characteristics. Specifically, we first investigate the impact of current widely used natural image augmentations on Mars images. Based on the analysis, we then proposed two novel and effective augmentations for SSL of Mars segmentation and augment instance normalization (AugIN) and SAM-Mix, which serve as strong augmentations to boost the model performance. Meanwhile, to fully leverage the unlabeled data, we introduce a soft-to-hard consistency learning strategy, learning from different targets based on prediction confidence. Experimental results show that our method can outperform state-of-the-art SSL approaches remarkably. Our proposed dataset is available at https://jhang2020.github.io/S5Mars.github.io/.**

***Index Terms*— Image semantic segmentation, Mars vision tasks, semi-supervised learning (SSL), terrain segmentation.**

I. Introduction

HUMANS have shown great enthusiasm for Mars. The history of human research on Mars dates back to the 1960s. So far, more than 30 rovers have been dispatched to the red planet, and the increasing amount of available data promotes the application and development of deep learning algorithms. Deep-learning-based methods have already assisted in prioritizing data selection [1], collecting data, and analyzing data [2], [3], [4]. This article explores the task of Mars terrain semantic segmentation, which aims to identify the drivable areas and the specific terrains from images. It is of great significance to obstacle avoidance, traversability estimation, data collection, and path planning [5], [6], ensuring the safety and productivity of ongoing and future missions to Mars.

Mars semantic segmentation faces problems from both data and method design. First, the lack of satisfactory and available data hinders the development of deep learning methods to some extent. On the one hand, because of the high cost of Mars rovers, limited bandwidth, and data transmission loss from Mars to Earth, collecting Martian data is very expensive. On the other hand, due to the complexity and similarity of the terrain, delicate and dense pixel-level labeling is highly specialized and time-consuming. Accordingly, previous datasets [7], [8] are not satisfactory because of the low-quality annotations or the roughly defined categories. AI4Mars [8], a newly published Mars terrain segmentation dataset, only defines four simple categories that are difficult to meet the actual requirements of complex terrain identification. Besides, some datasets [7], [8] collected through crowdsourcing often do not have satisfactory annotation quality due to inconsistent standards.

From a methodological point of view, the existing methods heavily rely on large amounts of training data and lack targeted and effective design. Early works directly applied a certain machine learning algorithm such as support vector machines (SVMs) [6]. With the rapid development of deep learning, the terrain segmentation performance is greatly improved by methods based on deep neural networks [5], [8], [9]. However, they still rely on fully supervised learning pipelines that require a lot of high-quality labeled data, which is often difficult to achieve. To this end, semi-supervised learning (SSL) has attracted lots of attention, which learns representations from limited labeled data and the amounts of unlabeled data. However, most existing SSL methods are designed for Earth image data and cannot be directly transferred to Mars image segmentation tasks due to the properties of Mars images. First, the color of Mars images is less diverse. Traditional color augmentations, which are crucial and widely used in SSL works [10], [11], [12], can cause overdistortion problem [13] in the form of color distribution shift for the Mars images and fail to improve the performance. Note that color distribution shifts can arise in different data domains with some similar properties as the Mars images, e.g.,

Manuscript received 8 February 2024; revised 25 March 2024; accepted 2 April 2024. Date of publication 16 April 2024; date of current version 22 April 2024. This work was supported in part by the National Key Research and Development Program of China under Grant 2018AAA0102702 and in part by the National Natural Science Foundation of China under Grant 62172020. *(Jiahang Zhang and Lilang Lin contributed equally to this work.) (Corresponding author: Jiaying Liu.)*

The authors are with the Wangxuan Institute of Computer Technology, Peking University, Beijing 100080, China (e-mail: zjh2020@pku.edu.cn; linlilang@pku.edu.cn; zejia@pku.edu.cn; daooshee@pku.edu.cn; liujiaying@pku.edu.cn).

Digital Object Identifier 10.1109/TGRS.2024.3386756

less diverse color distributions, when applying the traditional color augmentations. Nevertheless, it is still less explored in previous SSL works, especially from the perspective of data augmentations. Besides, the objects in Mars images are often with irregular contours and obvious occlusions, e.g., between rocks and soil/sand. As a result, the high background complexity makes the model suffer from greater uncertainty in the consistency learning of unlabeled data, leading to suboptimal representations. Moreover, some categories are more confusing between each other, e.g., rocks and bedrock, soil, and sand, which require more fine-grained representations to distinguish.

In summary, there are two main challenges in the Mars terrain segmentation task: 1) the lack of data with adequate detailed and high-confidence annotations and 2) insufficient studies targeted at SSL on Mars image data. We solve the above problems from the perspective of *both data and method design*, which are named semi-supervised semantic segmentation for Mars (**S^{5}Mars**). We first create a new dataset to provide high-quality and fine-grained labeled data for Mars terrain segmentation. Our dataset contains 6k high-resolution images captured on the surface of Mars, each of which is annotated by a professional team. There are nine categories defined in our dataset, including sky, ridge, soil, sand, bedrock, rock, rover, trace, and hole, respectively. To improve the quality of labels, the annotation of the dataset adopts a sparse labeling style, i.e., only the area with high human confidence is annotated.

To learn from these sparse data, we propose a new semi-supervised framework for Mars image terrain segmentation. Our method is based on the recently popular consistency regularization-based methods that utilize weak-to-strong augmentations to generate the perturbation while pursuing the perturbation consistency. Specifically, we first investigate the impact of widely used Earth image augmentations on Mars data and are surprised to find their adverse effects on the SSL of Mars segmentation. Based on this analysis, we further propose two novel and effective augmentations: augment instance normalization (AugIN) and SAM-Mix. AugIN exchanges statistics between images to generate new data views while avoiding drastic color distribution shifts. SAM-Mix utilizes the pretrained segment-anything model (SAM) [14] to generate high-quality object masks, reducing the uncertainty of the mixed images. These two data augmentations lead to better consistency in learning and improve performance remarkably. Finally, we introduce the soft-to-hard consistency learning strategy that utilizes the soft pseudolabels in low-confidence regions while using the hard pseudolabels in high-confidence regions, fully taking advantage of the unlabeled data. Extensive experiments and ablation studies verify the effectiveness of the proposed method.

Our contributions can be summed up as follows.

1) We collect a new fine-grained labeled Mars dataset for terrain semantic segmentation, which contains a large amount of Martian geomorphological data. Our dataset is sparsely annotated by a professional team under multiple rounds of inspection rework. The high-quality dataset can provide accurate and rich segmentation guidance.
2) We systematically study the data augmentations used in current mainstream SSL methods and find their detrimental impact on Mars image segmentation, especially the traditional color augmentations. We analyze this problem and further propose two new and effective augmentations, SAM-Mix and AugIN, boosting the performance of SSL methods for Mars image segmentation.
3) To fully take advantage of the unlabeled data, a soft-to-hard consistency learning strategy is introduced. The model is constrained to learn consistency by the hard pseudolabels in high-confidence regions and the soft pseudolabels in low-confidence regions, further improving the consistency.

The rest of this article is organized as follows. In Section II, we provide a detailed survey of Martian datasets and a brief review of deep learning for Mars. Section III introduces our proposed Mars segmentation dataset. Then, we present our framework for Mars semantic segmentation in Section IV. Experimental results and analysis are shown in Section V. The conclusion is finally given in Section VI.

II. Related Works

A. Deep Learning for Mars

With the increasing amount of available data and the rapid development of computing power, deep learning is playing an increasingly important role in Mars exploration.

For many reasons such as limited computing resources, existing deep learning methods are usually ex-situ (Earth edge). For terrain identification, Deep Mars [16] trains an AlexNet to classify engineering-focused rover images (e.g., those of rover wheels and drill holes) and orbital images. However, it can only recognize one object in a single image. The soil property and object classification (SPOC) [9] proposes to segment the Mars terrains in an image by using a fully convolutional neural network. Swan et al. [8] collect a terrain segmentation dataset and evaluate the performances using DeepLabv3+ [28]. Considering the dependence of existing methods on large amounts of data, Goh et al. [29] utilize a self-supervised method and train the model on less labeled images. Recently, the Transformer-based network has been studied [18], [30] for the Martian rock segmentation task. For other tasks, Zhang et al. [31] deal with the Mars visual navigation problem by utilizing a deep neural network, which can find the optimal path to the target point directly from the global Martian environment.

Meanwhile, intrigued by the vision of autonomous probes that rely on deep learning even without human-in-the-loop requirements, scientists are studying the potential of implementing in situ (Mars edge) deep learning algorithms using high-performance chips [32]. For example, the scientific captioning of terrain images (SCOTI) [1] model automatically creates captions for pictures of the Martian surface based on LSTM, which helps selectively transfer more valuable data within downlink bandwidth limitations. For energy-

TABLE I
SUMMARY OF MARS TERRAIN-AWARE DATASETS

Type	Source	Dataset	Scale	Classes	Description
Real	Curiosity rover	[9]	5k	-	Wheel slip and slope angles prediction
			700	6	Terrain segmentation
		[5]	300	3	Terrain classification
		[15]	620	4	Terrain classification
		[16]	6k	24	Terrain classification
		[17]	405	-	Rock detection
		[18]	8k	-	Rock detection
		[1]	1k	-	Image description
		[19]	310k	-	Compressed image quality evaluation with automatic labeling
	Opportunity, Spirit rovers	[20]	117	-	Rock detection
	Curiosity, Opportunity, Spirit rovers	[21]	46	2	Terrain segmentation
		[8]	35k	4	Terrain segmentation
		[22]	5k	9	Terrain segmentation
		[7]	5k	6 (17 sub)	Terrain segmentation
Real + Synthetic	Curiosity rover	[23]	30k	5	Terrain classification
Synthetic	ROAMS rover simulator	[20]	55	-	Rock detection
Simulation field	Atacama Desert Zoë rover prototype	[24]	30	-	Rock detection
	JPL Mars Yard FIDO rover Platform	[20]	35	-	Rock detection
	JPL Mars Yard Athena rover Platform	[25]	91k	-	Rover energy consumption
	Devon Island	[26]	400	-	Rock detection
Real + Simulation field	Opportunity, Spirit rovers	[27]	36	2	Terrain segmentation

optimal driving, Higa et al. [25] propose to predict energy consumption from images based on a PNASNet-5 [33].

However, many existing works still directly transfer the technology designed for the Earth scene to the Mars task, which can be suboptimal due to the properties of Mars data. Meanwhile, due to the significant bandwidth and computational resource limitations, the model is expected to be lightweight and efficient, and hence, the large models are unsuitable to employ. Most importantly, most of these methods require a lot of annotated training data, which is expensive and hard to obtain. Although some domain adaptation methods [22], [34] also can learn the target domain knowledge without many labels, they still suffer from taxonomy inconsistencies in segmentation detail, as discussed in [29] and [35]. To this end, in this article, we present a powerful SSL framework designed for the Mars images.

B. Datasets for Mars Vision

Datasets are the basis for intelligent algorithm development. At present, there are various datasets of planetary surfaces, such as the digital simulation Lunar landscape segmentation dataset ALLD. As for Mars, the commonly used terrain-aware datasets can be divided into three categories: rover shooting real data, artificial synthetic data, and Earth simulation field shooting data. The rover shooting data are captured by devices of rovers that land on Mars. The number of rovers sent to Mars will gradually increase along with the progress of space research. However, the amount of data available now is still relatively limited. Synthesizing Mars datasets by means of digital modeling simulation or adversarial learning is an important data supplement but can differ greatly from the real Mars data. Earth simulation field shooting way requires building a simulation platform or finding a similar landscape on Earth to Mars, which is difficult to implement. The current Mars terrain-aware datasets are shown in Table I, which are shot by the Mars rovers. A large proportion of them have an image quantity of less than 1000, which cannot meet the training needs of the machine learning models. The richness of Mars terrain-aware datasets still needs to be strengthened.

C. Semi-Supervised Learning

SSL [36] utilizes the manifold structure of unlabeled data to assist learning with labeled data. The key issue is how to exploit the information of unlabeled data. Generally, the cross-entropy loss is optimized by the ground-truth label on the labeled data, while a regularization term is applied to the model with respect to the unlabeled data. For example, the pseudolabel method [37] assigns pseudolabels to unlabeled data through a classifier trained on supervised data, which is typical in entropy minimization methods.

Regarding the utilization of unlabeled data, many researchers have conducted extensive studies, covering unsupervised contrastive learning [38], [39], uncertainty attention mechanism [39], [40], and extra correcting networks [41]. However, these methods improve the performance at the cost of increasing space and computational complexity. Recently,

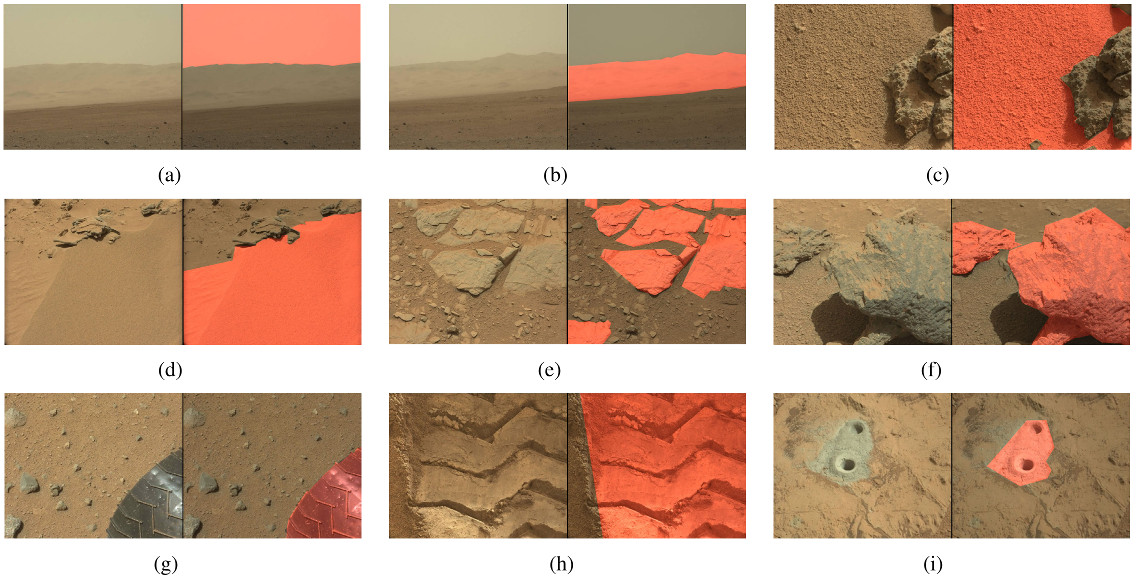
(a) (b) (c) (d) (e) (f) (g) (h) (i)

Fig. 1. Examples for each label category (highlighted in red). (a) Sky. (b) Ridge. (c) Soil. (d) Sand. (e) Bedrock. (f) Rock. (g) Rover. (h) Trace. (i) Hole.

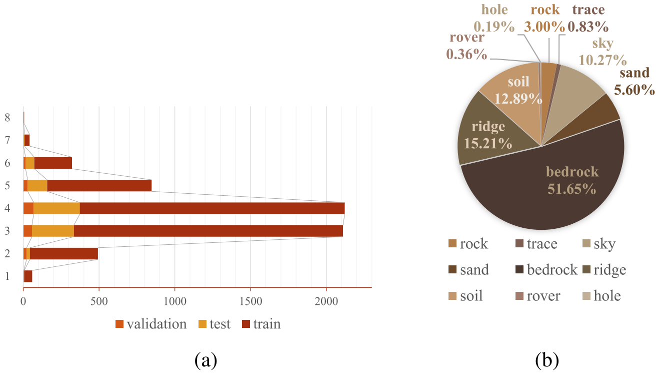

(a) (b)

Fig. 2. Numerical statistics on our S^{5}Mars dataset. The figures show the richness of the categories from two aspects: the distribution of the number of different labels in each image and the distribution of label area. Note that no image contains nine labels simultaneously in its annotation, so it is omitted in (a). (a) Number of images with n categories appearing simultaneously. (b) Distribution of different label areas.

consistency regularization-based methods have attracted lots of attention due to their simplicity and effectiveness. They rely on various perturbation techniques (augmentations) to generate different data patterns, which maintain similar semantic information as the original data. Then, the consistency regularization objective is performed to guide the learning of the unlabeled data. MixMatch [42] mixes labeled and unlabeled data using MixUp [43] and performs consistency regularization utilizing low-entropy labels. FixMatch [10] further assigns pseudolabels that are the predictions by the teacher model on weakly augmented data to the corresponding strongly augmented data. Inheriting from FixMatch, FlexMatch [44] and FreeMatch [45] propose to learn the threshold for different classes adaptively to filter the low-confidence pseudolabels. Zhao et al. [11] proposed a series of strong data augmentations to enhance the augmented space. UniMatch [12] utilizes both the data- and feature-level augmentations to constrain the consistency learning.

In these consistency regularization methods, the augmentations, i.e., the perturbation techniques, are crucial for the semantic segmentation. Many techniques, e.g., geometric-, color-, mixing-, and feature perturbation-based methods, have been studied. Furthermore, some random autoaugment modules are developed [46] to further expose data patterns. However, these methods are less suitable and effective for the Mars semantic segmentation due to the special properties of Mars images as we discussed in Section I. Therefore, it is significant and critical for the study of augmentations for Mars image data. In this article, we analyze the characteristics of Mars images and study the performance of existing common augmentations on Mars data. Meanwhile, we propose two effective new augmentations to boost SSL for Mars image segmentation.

III. Proposed Mars Imagery Segmentation Dataset

To solve the problem of scarce available training data for deep learning, we create a fine-grained labeled Mars dataset for the exploration on Mars surface, namely, S^{5}Mars. Our dataset includes 6000 high-resolution images taken on the surface of Mars, by a color mast camera (Mastcam) from Curiosity (MSL), with a spatial resolution of 1200 × 1200. The dataset is divided in a roughly stratified sampling manner to make the label distribution similar among different splits, yielding a training set of 5000 images, a validation set of 200 images, and a test set of 800 images.

A. Labeling Process

There are nine label categories: sky, ridge, soil, sand, bedrock, rock, rover, trace, and hole, respectively. Examples of each category are shown in Fig. 1. The labeling criteria are given as follows.

1) *Sky:* The Martian sky, often at the top of a distant image, bounded by the upper edge of a mountain or horizon.
2) *Ridge:* The distant peaks bounded by the sky above and the horizon below.
3) *Soil:* Unconsolidated or poorly consolidated weathered material on the surface of Mars, with larger and coarse-grained grains containing small stones.

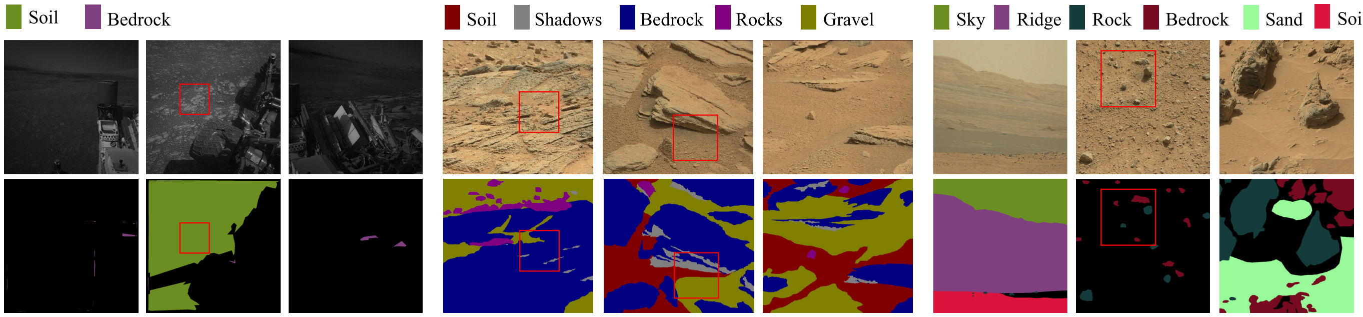

(a) (b) (c)

Fig. 3. Some image-label examples in different datasets. (a) AI4Mars [8]. Due to the few defined categories, the annotation diversity and adequacy are insufficient. Meanwhile, there are some cases of mislabeling (red box). (b) Mars-Seg [22], which gives complete pixel-level labeling. However, the label can be misleading when different categories mix up with each other (red box). (c) Our dataset S^{5}Mars, which provides accurate labeling for regions with high confidence.

4) *Sand:* Granular material, more fluid, less viscous, some with windward and leeward sides, and most of the time with sand ridges.
5) *Bedrock:* Partially covered by the soil and buried at varying depths.
6) *Rock:* A stone that is completely exposed to the ground and is roughly lumpy or oval in shape, usually with distinct shadows.
7) *Rover:* The rover itself.
8) *Trace:* The trace left by the rover when it passed over the ground.
9) *Hole:* The hole left by the rover during its sampling operation on Mars, contains the surrounding soil of different colors.

Martian surface conditions are complicated due to the harsh and volatile Martian environment. The terrain types can mix and overlap with each other, and it becomes hard for humans to distinguish the correct categories clearly. Considering the situation, we apply *sparse labeling*, i.e., only the pixels with enough human confidence are labeled. The overall annotation priority is in a coarse-to-fine manner, which means that we label each image in order of object size, and the total pixel annotation ratio is 48.9%. As for the annotating process, the annotation rules are discussed more than ten times to keep consistency and preciseness. Each annotation result passes more than two turns of quality inspections. Annotation work is carried out by a professional team, where 90% of the annotators have been engaged in such annotation work more than six times. The annotation time of each terrain image is about 30 min.

B. Comparison and Analysis

We make a statistical analysis of the semantic labels in the dataset, as shown in Fig. 2. We show the distribution of the number of different labeled categories contained in each image in Fig. 2(a). Most images are relatively complex with three or four annotations in one scene. This distribution on training, validation, and test sets keeps good consistency.

We make statistics of the distribution of label area of each category, as shown in Fig. 2(b). The total pixelwise label ratio is 49%. The category, bedrock, has the largest annotation number while the category of ridge is the second. Rocks appear in most of the images in the dataset, but the total area is small. The artificial impact, e.g., rover, trace, and hole, accounts for few portions of the labeled area, but they have a greater variety of shapes and are crucial to the observation and judgment system for intelligence research on Mars.

AI4Mars contains four categories with gray-scale images available solely, which can only provide limited task knowledge. Moreover, since AI4Mars is a crowdsourcing project, though the number of submissions is large, the annotators may have inconsistent understandings of labeling standards, which can lead to mislabeling in the annotations, as shown in Fig. 3(a). In contrast, our dataset is equipped with high-resolution RGB images, including nine semantic categories. Meanwhile, we establish clear labeling criteria and provide professional training to annotators, making the proposed dataset more reliable.

Mars-Seg [22] is also a public Mars terrain segmentation dataset. The dataset has 1064 high-resolution gray-scale images and 4184 RGB images with a spatial resolution of 560 × 500, while S^{5}Mars is composed of high-resolution RGB images, which offers more accurate and more abundant semantic information for detection and segmentation tasks. Meanwhile, categories in Mars-Seg such as gravel, sand, and rocks mix up with each other, making it hard to determine the terrain scene into any one category, as shown in Fig. 3(b). Instead, S^{5}Mars applies a confidence-based sparse-labeled manner. This way we guarantee that the labels are strongly representative in each category and reduce the label noise introduced in the labeling work, as shown in Fig. 3(c).

IV. Proposed Method

In this section, we introduce the proposed method for Mars image semantic segmentation. The overview and motivations are first provided in Section IV-A. Then, we systematically investigate the augmentations for Mars images in Section IV-B and propose two effective augmentation techniques based on the analysis. Finally, in Section IV-C, we introduce the soft-to-hard consistency learning strategy and present the full model.

A. Preliminaries and Motivation

1) Overview: As introduced in the previous sections, our proposed dataset is annotated in a sparse style, i.e., some areas of an image are annotated and some are not. For clarity, we no longer distinguish between unlabeled images and unlabeled areas in an image, which can be aligned with a few minor changes. Following the dominant consistency regularization semi-supervised methods [10], [36], the model is trained on both labeled and unlabeled images simultaneously. Given a batch of labeled images $\mathcal{B}_l = \{(\mathbf{x}_i, \mathbf{y}_i)\}_{i=1}^{|\mathcal{B}_l|}$ and a batch of unlabeled images $\mathcal{B}_u = \{(\mathbf{u}_i)\}_{i=1}^{|\mathcal{B}_u|}$, the goal of SSL is to train a model $f(\cdot;\theta)$ with good representations by optimizing the following objective $\mathcal{L}$:

$$\mathcal{L} = \mathcal{L}_{\text{sup}} + \lambda_u \mathcal{L}_{\text{unsup}} \tag{1}$$

where $\mathcal{L}_{\text{sup}}$ is the supervised loss on the labeled images, i.e., the cross-entropy loss, and the $\mathcal{L}_{\text{unsup}}$ is the unsupervised loss for unlabeled images. λ_u controls the weight of unsupervised term.

Our method is based on the recent popular consistency regularization-based SSL method, FixMatch [10]. Specifically, a two-branch network is adopted, consisting of a teacher model $f(\cdot;\theta_t)$ and a student model $f(\cdot;\theta_s)$. The teacher model $f(\cdot;\theta_t)$ can be identical to the student model sharing the same weights. Alternatively, it can be updated gradually via the exponential moving averaging (EMA) of the student model weights

$$\theta_t \leftarrow m\theta_t + (1-m)\theta_s \tag{2}$$

where $m \in [0, 1)$ is the momentum coefficient. We follow the EMA setting to update the teacher model, which is also recommended in mean-teacher [47]. The student model is optimized via the backward gradients.

The core implementation in FixMatch is the weak-to-strong augmentation strategy, which serves as the perturbations and generates different augmented data views. Specifically, given the weak augmentations $\mathcal{T}_w$ and strong augmentations $\mathcal{T}_s$, the augmented views $\mathbf{u}_i^w = \mathcal{T}_w(\mathbf{u}_i)$ and $\mathbf{u}_i^s = \mathcal{T}_s(\mathbf{u}_i)$ are constructed and fed into the teacher and student models to encode, respectively. The teacher model assigns the pseudolabels for weakly augmented images, which are then utilized in the learning of the student model for strongly augmented images. Concretely, the unsupervised consistency loss can be formulated as follows:

$$\mathcal{L}_{\text{unsup}}^{\text{ce}} = \frac{1}{|\mathcal{B}_u|}\sum_{i=1}^{|\mathcal{B}_u|}\frac{1}{H\times W}\sum_{j=1}^{H\times W}\mathcal{L}_{\text{ce}}\big(\mathbf{p}_i^s(j), \mathbf{y}_i^t(j)\big) \tag{3}$$

$$\mathbf{y}_i^t(j) = \mathbb{1}\big(\text{argmax}(\mathbf{p}_i^t(j))\big) \tag{4}$$

where $\mathbf{p}_i^s(j)/\mathbf{p}_i^t(j)$ is the predicted scores output by the student/teacher model after the softmax layer corresponding to the j_{th} pixel of the i_{th} unlabeled image $\mathbf{u}_i$. $\mathbf{y}_i^t(j)$ is the one-hot encoding of the pseudolabel generated from the teacher model, and $\mathbb{1}$ is the one-hot indicator function. H and W are the height and width of the image. $\mathcal{L}_{\text{ce}}$ is the cross-entropy loss function.

2) Motivation: For SSL in Mars image semantic segmentation, there are two main challenges to be solved: 1) previous augmentations for the natural images on Earth can be ineffective due to the different properties of Mars images and 2) unlabeled regions of the Mars images tend to be with high uncertainty, making the pseudolabels less reliable for training. These problems affect the performance of the existing SSL frameworks for Mars image segmentation. To overcome these challenges, we propose a simple yet effective SSL framework, as shown in Fig. 4, which adopts effective augmentations and learns semantic representations by exploring soft-to-hard consistency, which will be introduced in the following parts.

TABLE II

COMPARISON OF THE STATISTICAL INFORMATION BETWEEN THE MARS IMAGES AND EARTH IMAGES. LOWER VALUES OF THE METRICS INDICATE LESS DISPERSION OF THE DATA DISTRIBUTION

Dataset	(R, G, B)	
	Standard Deviation	Variable Coefficient
S^{5}Mars	(0.134, 0.121, 0.099)	(0.214, 0.233, 0.273)
ImageNet [52]	(0.229, 0.224, 0.225)	(0.472, 0.491, 0.554)

B. Augmentations for Mars Images

As pointed in previous works [10], [11], [12], the augmentation module plays an important role in SSL, encouraging the model to learn the consistency in the perturbations. Generally, the common augmentations adopted for SSL methods can be divided into the following categories.

1) *Geometrical Augmentation:* It utilizes some geometrical transformations, e.g., *flip* and *translate*, to generate new data views. These augmentations often serve as the basic augmentations, i.e., the weak augmentations, due to their efficiency and stability.
2) *Noise-Based Augmentation:* Different augmented views can be obtained by simply injecting random noise into the original image, e.g., *Gaussian noise*, and *random mask*.
3) *Color-Based Augmentation:* A series of color transformations are introduced to further enlarge the data distributions, e.g., *Gaussian blur*, *equalize*, and *sharpness*. More details can be found in [46]. These transformations facilitate the model to learn the intrinsic semantic consistency by perturbing the color distribution of images.
4) *Mixing-Based Augmentation:* Mixing methods have been proven effective for SSL scenarios. They mix the two samples via the interpolation (Mixup [43]) or cut-paste (CutMix [48]) operations. Some advanced mixing methods are further developed for SSL such as CowMix [49] and ClassMix [50].
5) *Feature-Level Augmentation:* The most common augmentation in feature-level is the *dropout* [51] operation, which can also be regarded as a kind of model perturbation. It is often utilized as strong augmentations in conjunction with other augmentations.

We focus on the latter four, which serve as strong augmentations and have a significant impact on model performance. Following the recent work [11], we adopt *resize*, *crop*, and *flip* as the weak augmentations. In addition, we choose different augmentations, which are commonly used

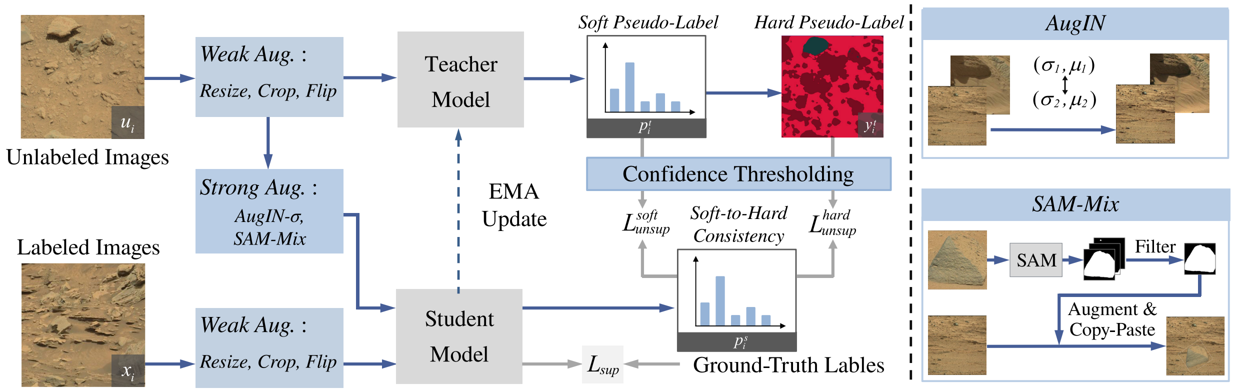

Fig. 4. Overview of the proposed framework for semi-supervised Mars semantic segmentation. We adopt a two-branch teacher–student architecture. Two novel augmentations are proposed as strong augmentations: AugIN and SAM-Mix. AugIN exchanges the statistics of the two samples, i.e., mean and standard deviation. SAM-Mix utilizes an off-the-shelf SAM to obtain the object binary masks to perform copy-paste operations, reducing the uncertainty of the augmented images. Finally, the model is optimized according to a soft-to-hard consistency learning strategy, utilizing both the soft labels $\mathbf{p}_i^t$ and the hard labels $\mathbf{y}_i^t$ based on the confidence.

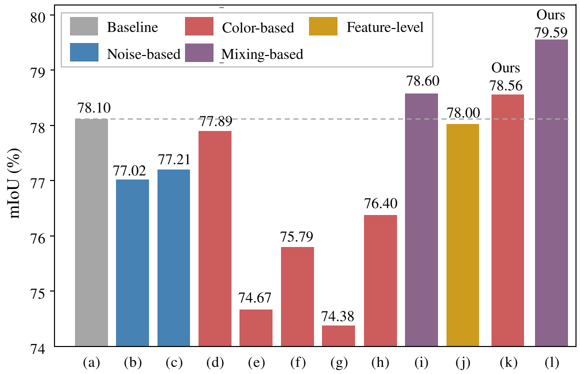

Fig. 5. Comparison of different augmentations on SSL for Mars segmentation. (a) Identity. (b) Gaussian noise. (c) CutOut. (d) Gaussian blur. (e) Hue. (f) Contrast. (g) Equalize. (h) Brightness. (i) CutMix. (j) Dropout. (k) and (l) Proposed AugIN and SAM-Mix.

and found beneficial for the learning of Earth images, as strong augmentations to demonstrate their impact separately. The results are shown in Fig. 5. As we can see, unlike natural images on Earth, the noise- and color-based and feature augmentations cannot bring a boost compared with the "identity" baseline. To further understand this phenomenon, we analyze the data from a statistical perspective and present the comparison of standard deviation and coefficient of variation between Mars and Earth images. As shown in Table II, the dispersion of RGB values in the Mars image is much less than that of the Earth natural image, which indicates that the color distribution of the Mars image is more concentrated. It is in line with our observation that there is a high similarity within and between Mars images. Based on this conclusion, we argue that the traditional color-based perturbations lead to the color distribution shift of Mars images, causing the overdistortion problem [13], as shown in Fig. 6, which is not conducive to the model segmentation learning. Note that this is not trivial in the context of SSL because most previous SSL works adopt color augmentations as a strong technique by default and lack specific consideration on the Mars images. Meanwhile, we empirically find that the feature perturbation dropout also fails to improve the performance because it does not generate new input samples and cannot help the model learn richer semantic information. Besides, due to the irregular objects with occlusions and unclear contours, the model can face more serious uncertainty and consistency learning difficulty under the noise-based and random mixing-based augmentations, which will be discussed in the following.

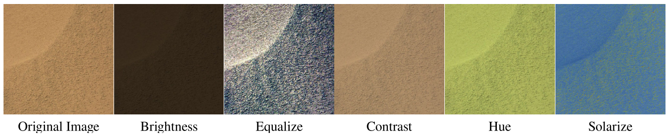

Fig. 6. Examples of color-based augmented images. More details of the augmentations can be found in [46].

To this end, we propose two effective augmentations designed for Mars images, AugIN and SAM-Mix, and employ them in our method to boost the SSL performance.

1) AugIN: To avoid drastic changes in image color distribution caused by direct perturbation, we propose AugIN that generates augmented data views by exchanging statistics of different images, i.e., the mean and standard deviation. This is inspired by the successful practice of style transfer [53]. Specifically, given an image $\mathbf{u}_i$ and a randomly sampled image $\mathbf{u}_j$, we exchange the mean and standard deviation as follows:

$$\text{AugIN}(\mathbf{u}_i, \mathbf{u}_j) = \sigma\left(\mathbf{u}_j\right)\left(\frac{\mathbf{u}_i - \mu(\mathbf{u}_i)}{\sigma(\mathbf{u}_i)}\right) + \mu(\mathbf{u}_j) \qquad (5)$$

where $\mu(\cdot)$ and $\sigma(\cdot)$ are the mean and standard deviation functions. Meanwhile, we can spontaneously obtain the two variants, AugIN-μ and AugIN-σ, which only exchange the mean or standard deviation between two samples. In the implementation, we exchange the image statistics within the same batch following a randomly generated permutation. Note that the operation in our method that exchanges the statistics of images within the same batch does not change the statistics of the entire batch, which can be theoretically verified easily. This stabilizes the color distribution after augmentation and generates more reasonable augmented data. In contrast, traditional color augmentations change the statics directly without considering the whole color distribution, making the model suffer from the potential color distribution shift problem.

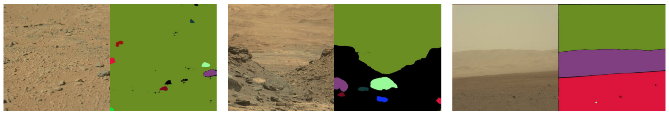

Fig. 7. Examples of image–mask pairs. We show the filtered masks of each image with high predicted confidence. Note that these masks are output by SAM in an instancewise manner, and we illustrate them in different colors.

2) SAM-Mix: As shown in Fig. 5, CutMix achieves a modest performance gain over the baseline, failing to meet the expected level of improvement. This is because there are many fragmentary objects with unclear edges in Mars images, and a random cut-pasting manner may lead to high uncertainty, limiting the model's performance. To this end, we propose SAM-Mix, which is formulated as a generalization of CutMix using binary mask output by an off-the-shelf SAM [14].

SAM attracts lots of attention recently, which can produce binary masks for the objects in an image from input or randomly generated prompts. We utilize an off-the-shelf SAM to produce a mask of the target object and paste it into the source image. Compared with random rectangular mask generation, SAM can generate high-quality masks to segment specific objects, as shown in Fig. 7. Specifically, given an image, a list of binary masks with the corresponding confidence score is output by SAM. These masks are first filtered so that: 1) the size of the mask is limited to a certain range and 2) the confidence of the mask is above a certain threshold. If there is no qualified mask, a random rectangular mask will be directly generated. Then, a Gaussian filter is applied to the masks to eliminate possible noise. Subsequently, we randomly select a qualified mask and further transform the masked object, i.e., *rotation*, *flip*, and *rescaling*. The pasting position will not be adjusted, that is, it will generally pasted corresponding to the position of the original image to avoid some unreasonable cases, e.g., the sky appearing in the bottom half of the image. The corresponding segmentation labels are also generated in the same way, which is used to train the model as previous work [54].

We note that textitSAM-Mix shares similarities with other segmentation-based mixing augmentation strategies [50], [55], [56], [57], [58], which develop the binary mask generation in an instancewise or classwise manner. However, in contrast to the above mixing methods, SAM-Mix gets rid of the reliance on ground-truth labels, making it possible for the augmentation of unlabeled images. Furthermore, SAM's strong generalization ability enables us to produce high-quality masks for individual objects efficiently, which is compatible with images of Mars that contain multiple objects simultaneously. SAM-Mix reduces the uncertainty caused by random mixing and further improves the performance of the model.

C. Soft-to-Hard Consistency Learning

As mentioned in Section I, the Mars images are with more confusing categories, such as sand and soil, rock and bedrock, which require a more fine-grained representation learning target, especially for the unlabeled regions with high uncertainty in our dataset. Meanwhile, for the data collection and annotation, it is more difficult to obtain large-scale and high-quality annotated Mars images than natural Earth images due to the complexity of the Mars terrain, the required expert knowledge, and the limited transmission bandwidth. Therefore, previous works using only unlabeled regions with high confidence for training can be suboptimal in the Mars SSL context.

To this end, we propose a soft-to-hard consistency learning strategy that utilizes both the soft and hard pseudolabels according to a confidence thresholding policy. The hard pseudolabel is the one-hot label representation $\mathbf{y}_i^t(j)$ in (3), which is obtained by the argmax$(\cdot)$ operation. The soft label is represented as the model prediction scores $\mathbf{p}_i^s(j)$, which denotes the probability distribution over different semantic categories. Specifically, the optimization objective for the soft pseudolabel can be formulated as

$$\mathcal{L}_{\text{unsup}}^{0} = -\frac{1}{|\mathcal{B}_u|}\sum_{i=1}^{|\mathcal{B}_u|}\frac{1}{H\times W}\sum_{j=1}^{H\times W}\mathbf{p}_i^t(j)\log\bigl(\mathbf{p}_i^s(j)\bigr). \quad (6)$$

Intuitively, (6) optimizes the similarity of the two distributions, i.e., p_i^t and p_i^u, which indicate the predicted class probability of the teacher and student models. Based on this objective, we can further find the following.

1) When $\max(\mathbf{p}_i^t(j)) \approx 1$, the teacher model assigns the pseudolabels with high confidence, and(6) degenerates to be almost equivalent to (3).
2) When $\max(\mathbf{p}_i^t(j)) < 1-t$ where t is a positive constant, the predictions of the teacher model are less confident. This objective encourages the student model to learn the consistency measured by the relevance of current features to different prototype anchors. This can be seen as a more fine-grained smooth label of the unknown regions in Mars images, which can belong to a new class or the old class with high uncertainty.

Therefore, the hard label provides a confident target to force the model to predict a distribution with low entropy, learning the explicit semantic mapping in images. In contrast, the soft label objective encourages the model to learn the consistency in a more gentle way, which can be viewed as performing the self-distillation [59] of relational knowledge, modeled as the feature similarity to the prototype features stored in the weights of the classification head. This allows the model to make better use of unlabeled data to improve the representation consistency learning in an unsupervised manner, achieving a better representation space.

Based on the above analysis, we propose a confidence-based thresholding policy to integrate the two objective functions organically. We utilize the hard pseudolabels in high-confidence regions while using soft pseudolabels in low-confidence regions, fully taking advantage of the training signals from unlabeled data. Specifically, we first obtain the confidence score of teacher model predictions as $\max(\mathbf{p}_i^t(j))$. Then, the student model is optimized as follows (t_{hard} and t_{soft} are the threshold hyperparameters).

1) If $\max(\mathbf{p}_i^t(j)) > t_{\text{hard}}$, (3) is applied to optimize the model with the highly confident one-hot pseudolabel;

TABLE III

SEGMENTATION PERFORMANCE ON THE S^{5}MARS USING THE RESNET-50 AS THE BACKBONE

Method	20% data		50% data		100% data	
	mAcc (%)	mIoU (%)	mAcc (%)	mIoU (%)	mAcc (%)	mIoU (%)
Supervised	76.71	66.26	80.17	72.65	82.12	75.04
MT [47]	76.89	70.92	81.95	75.93	82.32	77.87
MT [47] + ClassMix [50]	77.38	71.54	82.34	76.42	83.21	78.04
FixMatch [10]	77.80	71.08	79.47	72.98	80.75	73.69
RanPaste [61]	76.36	66.66	80.51	74.08	82.28	75.78
U^{2}PL [38]	78.03	72.32	82.29	77.56	83.41	78.60
AugSeg [11]	78.28	72.38	81.52	75.40	81.82	76.90
UniMatch [12]	76.92	69.83	78.53	71.56	79.82	72.60
Ours	**82.85**	**76.49**	**83.56**	**78.66**	**84.73**	**80.15**

2) If $\max(\mathbf{p}_i^t(j)) < t_{\text{soft}}$, the soft label objective is optimized to avoid noisy signals from other prototype features in the high confidence region.

Finally, the model is optimized in an end-to-end manner using the objective in (1). The supervised term $\mathcal{L}_{\text{sup}}$ is the cross-entropy loss on the labeled images. The whole consistency regularization term $\mathcal{L}_{\text{unsup}}$ is

$$\mathcal{L}_{\text{unsup}} = \mathcal{L}_{\text{unsup}}^{\text{hard}} + \lambda_s \mathcal{L}_{\text{unsup}}^{\text{soft}} \tag{7}$$

where $\mathcal{L}_{\text{unsup}}^{\text{hard}}$ is exactly the $\mathcal{L}_{\text{unsup}}^{\text{ce}}$ in (3) and λ_s is the weight coefficient.

V. EXPERIMENTS AND RESULTS

A. Dataset

We use the proposed S^{5}Mars dataset and AI4Mars dataset that are introduced in Section III. For SSL evaluation, we adopt a stratified sampling strategy to extract different proportions of data from the dataset as labeled data and the rest as unlabeled data to jointly train our model. Note that all methods are evaluated under the same data partition lists.

B. Implementation Details and Metrics

Our model is based on DeepLabV3+ [28], adopting a ResNet-50 [60] pretrained on Image-Net [52] as the segmentation backbone. We use an output stride of 16 by default. The batch size is set to 8. A SGD optimizer with a momentum of 0.9 is adopted. A polynomial learning-rate decay with an initial value of 0.01 is adopted to train the student model. Specifically, the learning rate is scaled by $(1 - \text{iter}/\text{max\_iter})^{0.9}$. The EMA momentum coefficient m is set as $\min(1 - 1/(\text{iter} + 1), 0.996)$ following [11]. λ_r and λ_{unsup} are set to 1.0 and 2.0 by default. The model is trained for 240 epochs by default, and the teacher model is used for the evaluation. The images for training are cropped to the size of 512 × 512. The test images are center-cropped to 1024 × 1024 size. We train our model on a single NVIDIA RTX 3090 GPU.

We evaluate performance using *mean pixel accuracy* (mAcc) and *mean intersection over union* (mIoU) as the metrics.

TABLE IV

SEGMENTATION PERFORMANCE ON THE AI4MARS

Method	20% data		100% data	
	mAcc	mIoU	mAcc	mIoU
Supervised	71.68	66.14	74.43	68.34
MT [47]	75.44	70.13	77.82	71.98
MT [47]+ClassMix [50]	76.86	70.49	78.56	72.67
FixMatch [10]	76.27	70.36	77.37	71.90
RanPaste [61]	75.16	70.37	77.39	70.59
U^{2}PL [38]	77.11	70.89	78.62	72.41
AugSeg [11]	76.88	70.15	77.45	72.34
UniMatch [12]	75.60	70.24	77.21	71.36
Ours	**77.60**	**71.79**	**80.33**	**74.68**

C. Comparison Results

1) Compared With the SSL Methods: We compare our model with state-of-the-art SSL methods, Mean Teacher [47] (MT), ClassMix [50], FixMatch [10], RanPaste [61], U^{2}PL [38], AugSeg [11], and UniMatch [12], covering the latest consistency regularization-based and contrastive learning-based methods, as well as the naive supervised training results, which only utilize the labeled data. We implement these methods using their official codes (except for the MT which we adopt better training hyperparameters for fairness), using the same backbone ResNet-50. As shown in Tables III and IV, our method achieves the best performance across different labeled data ratios and datasets. MT [47] uses Gaussian noise and dropout as augmentations for both teacher and student branches. However, earlier works do not use a weak-to-strong augmentation strategy, which makes them suboptimal. We also employ the ClassMix [50] augmentation with MT. However, the quality of the generated mixed image strongly depends on the quality of the pseudolabels, which cannot be guaranteed on the Mars images with unclear object contours. FixMatch [10] and UniMatch [12] perform even worse than the supervised baseline when more labeled data are available. This is mainly because they employ a shared encoder instead of the teacher–student architecture, which we find less effective in our setting. Besides, AugSeg [11] achieves state-of-the-art performance on Earth image benchmarks, while it is not satisfying in the Mars semantic segmentation task due to the adopted various color augmentations. As for the contrastive

TABLE V

SEGMENTATION PERFORMANCE OF DIFFERENT CLASSES ON THE S^{5}MARS USING ALL LABELED TRAINING DATA

Method	Class IoU (%)									mIoU
	Sky	Ridge	Soil	Sand	Bedrock	Rock	Rover	Trace	Hole	
FixMatch [10]	88.97	90.06	83.05	74.19	92.09	20.31	52.54	88.75	73.26	73.69
U^{2}PL [38]	94.86	93.25	85.80	81.02	92.18	23.55	93.77	78.06	64.96	78.60
AugSeg [11]	94.75	93.00	84.78	77.36	92.02	10.33	83.08	81.00	75.84	76.90
Ours	95.64	94.20	87.18	83.18	92.42	22.89	87.17	85.60	74.10	**80.15**

TABLE VI

COMPARISON WITH THE ZERO-SHOT MODELS ON S^{5}MARS DATASET

Methods	mAcc (%)	mIoU (%)	Inference Time
SAM-CLS [14]	36.38	28.53	691 ms/img
SAN [62]	14.70	3.28	102 ms/img
SAN-FT [62]	11.60	10.54	102 ms/img
Ours	**84.73**	**80.15**	19 ms/img

learning-based methods, U^{2}PL uses filtered pseudolabels to perform pixelwise contrastive learning. However, the training cost of such methods is generally high, which will be discussed in Section V-D.

We also present the segmentation performance of each class in Table V. Note that the optimal data augmentations and learning strategy may differ across different categories. Remarkably, our method can achieve the best results in the head classes. Meanwhile, the performance on the tail classes, of which the sample number is small, is also comparable with other methods.

2) Compared With Zero-Shot General Models: Recently, the general large models for segmentation have achieved great success, which can deal with unseen data in training with the help of massive amounts of training data or the help of the vision-language model, e.g., CLIP [63]. Here, we highlight that current zero-shot learning methods or open-vocabulary methods are still unable to handle the Mars image semantic segmentation task well due to the fine-grained feature classification and required expert knowledge.

SAM [14] can produce high-quality object binary masks. To obtain the corresponding label, we apply a classification head subsequent to the image encoder. Specifically, the pretrained image encoder in SAM is fixed, and we train a classification decoder that takes the encoded feature as input and outputs the pixelwise semantic label, denoted by SAM-CLS. We can find that the extracted features by the encoder are not discriminative for Mars semantic segmentation, as shown in Table VI. As for vision-language models, we compare them with the state-of-the-art method, SAN [62]. We evaluate the model with both official model weights and fine-tuned weights on the target dataset, denoted as SAN-FT. However, poor performance is observed, as shown in Table VI. This is mainly due to two aspects: 1) the Martian terrain category is relatively rare in the corpus and 2) domain-specific expert knowledge is required for the fine-grained classification, which leads to the difficulty of feature space alignment for the Mars segmentation dataset. Moreover, their high training and inference overhead makes them suboptimal for resource-constrained extraterrestrial tasks.

Overall, our method achieves remarkable performance, which verifies the effectiveness of the proposed method.

TABLE VII

ABLATION STUDIES ON AUGIN. IDENTITY DENOTES THE METHOD WITHOUT AUGIN

Method	mAcc	mIoU
Identity	84.20	79.59
EFDM [64]	83.97	78.78
WCT [65]	83.38	78.83
FDA [58]	84.20	78.70
AugIN-μ	83.64	78.88
AugIN-σ	**84.73**	**80.15**
AugIN	83.58	78.69

TABLE VIII

ABLATION STUDIES ON DIFFERENT MIXING METHODS. IDENTITY DENOTES THE METHOD WITHOUT ANY MIXING AUGMENTATION

Method	mAcc	mIoU
Identity	83.33	78.56
CutMix [48]	83.85	78.98
ClassMix [50]	83.81	78.89
DACS [66]	83.80	78.69
SAM-Mix (Ours)	**84.73**	**80.15**

TABLE IX

ABLATION STUDIES ON THE OBJECT AUGMENTATIONS IN SAM-MIX

Flip	*Rotate*	*Rescaling*	mAcc (%)	mIoU (%)
			84.57	79.46
✓			**84.81**	79.71
✓	✓		84.80	79.88
✓	✓	✓	84.73	**80.15**

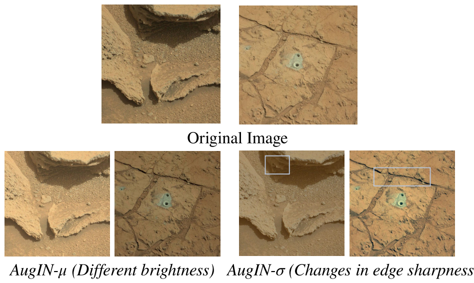
Original Image
AugIN-μ (Different brightness)
AugIN-σ (Changes in edge sharpness)

Fig. 8. Examples of augmented results by AugIN. AugIN-μ mainly affects the image brightness, while AugIN-σ changes the sharpness of the object edges.

TABLE X
ABLATION STUDIES ON SOFT AND HARD PSEUDOLABELS

Soft Label	Hard Label	mAcc (%)	mIoU (%)
✓		83.36	78.12
	✓	84.28	79.70
✓	✓	**84.73**	**80.15**

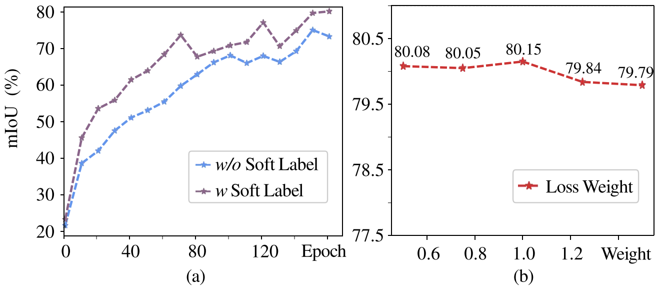

Fig. 9. (a) Effect of soft pseudolabels on the performance of different epochs. Faster convergence is observed when equipped with soft labels. (b) Ablation study results on the loss weight of soft pseudolabels.

TABLE XI
ABLATION STUDY ON THE THRESHOLD t_{HARD}

t_{hard}	mIoU (%)
0.9	78.82
0.7	79.31
0.6	79.87
0.5	**80.15**
0.4	80.00

TABLE XII
ABLATION STUDY ON THE THRESHOLD t_{SOFT}

t_{soft}	mIoU (%)
1.0	79.83
0.95	79.75
0.9	**80.15**
0.8	80.04
0.6	79.58

D. Ablation Studies

In the following, we conduct a series of ablations studies on the S^{5}Mars dataset using full data by default. ResNet-50 is adopted as the backbone.

1) Effect of AugIN: Recall that AugIN exchanges the mean or standard deviation of different samples, as shown in Fig. 8. First, we give the ablation studies on the different variants of the AugIN in Table VII. AugIN-μ, AugIN-σ, and AugIN denote swapping the mean, standard deviation, and both, respectively. As we can see, AugIN-σ can bring a boost to the model performance, while swapping the mean shows the adverse effect. By comparing the performance of different categories, we find that the main performance degradation comes from the hole, rover, and rock. We argue that this is because the mean of an image corresponds to the brightness. Exchanging the mean can cause inappropriate brightness changes in objects. For example, the brightness of a rover is obviously different from that of a rock, and corrupting this information is not conducive to distinguish objects. In contrast, the standard deviation mainly affects the degree of dispersion of the data while maintaining the overall brightness, which is mainly reflected in the clarity of the object edge. This helps the model to produce better prediction results at the object edge. We finally choose AugIN-σ in implementation.

Besides, to give a comprehensive evaluation, we provide the results of replacing AugIN with other methods [58], [64], [65] that exchange interimage information. FDA [58] exchanges low-frequency information, which is similar to AugIN-μ. Other style-transfer-based methods, i.e., EFDM [64] and WCT [65], also fail to improve the performance because they still cannot avoid the caused color distribution shift.

2) Effect of SAM-Mix: Table VIII gives the analysis of the SAM-Mix augmentation. The main difference between these approaches lies in the way the masks are generated. However, these generated masks have high uncertainty, making it difficult for the model to learn consistency in SSL tasks. CutMix randomly generates a rectangular mask from the beta distribution. ClassMix takes the predicted region of a certain category as the mask through the generated pseudolabels, while DACS uses the ground-truth labels to mix images. However, these methods are performed classwise instead of instancewise. For example, all rocks would be cut and pasted to another image, which can cause serious occlusions and increase the difficulty of consistency learning. Meanwhile, ClassMix, which relies on pseudolabels, still cannot provide good guidance in the early stage of training, while DACS, which is based on ground-truth labels, heavily relies on the number of labels and can only generate limited mixed samples. In contrast, we utilize the mask output by SAM to locate the objects and filter out the mask with higher confidence, achieving better performance.

Meanwhile, we present the effect of the objectwise augmentations, i.e., rotation, flip, and rescaling for the cutout object. As shown in Table IX, these simply available geometrical object augmentations can bring further improvement slightly by promoting mask diversity.

3) Soft-to-Hard Pseudolabel: To depict the semantic features in a more fine-grained manner, we utilize the soft pseudolabels in addition to the hard labels for the unlabeled images. Table X shows the effect of the soft and hard labels, respectively. As we can see, the model gives the best results when both kinds of labels are utilized. We note that only employing the soft labels cannot yield a good performance, which illustrates that the hard label is important for its low entropy constraints on the model output predictions. On the other hand, soft labels serve as a useful complement to hard labels, especially by making full use of the supervised signals in low-confidence regions. It promotes consistency learning by using the correlation between features and prototypes of different categories as the objective, which can be deemed as a relational knowledge distillation process.

Meanwhile, we note that the dual label optimization strategy can significantly improve the convergence speed of the model, as shown in Fig. 9(a). This is because of the extra supervisory signal provided by those low-confidence regions, which would be discarded using the hard labels.

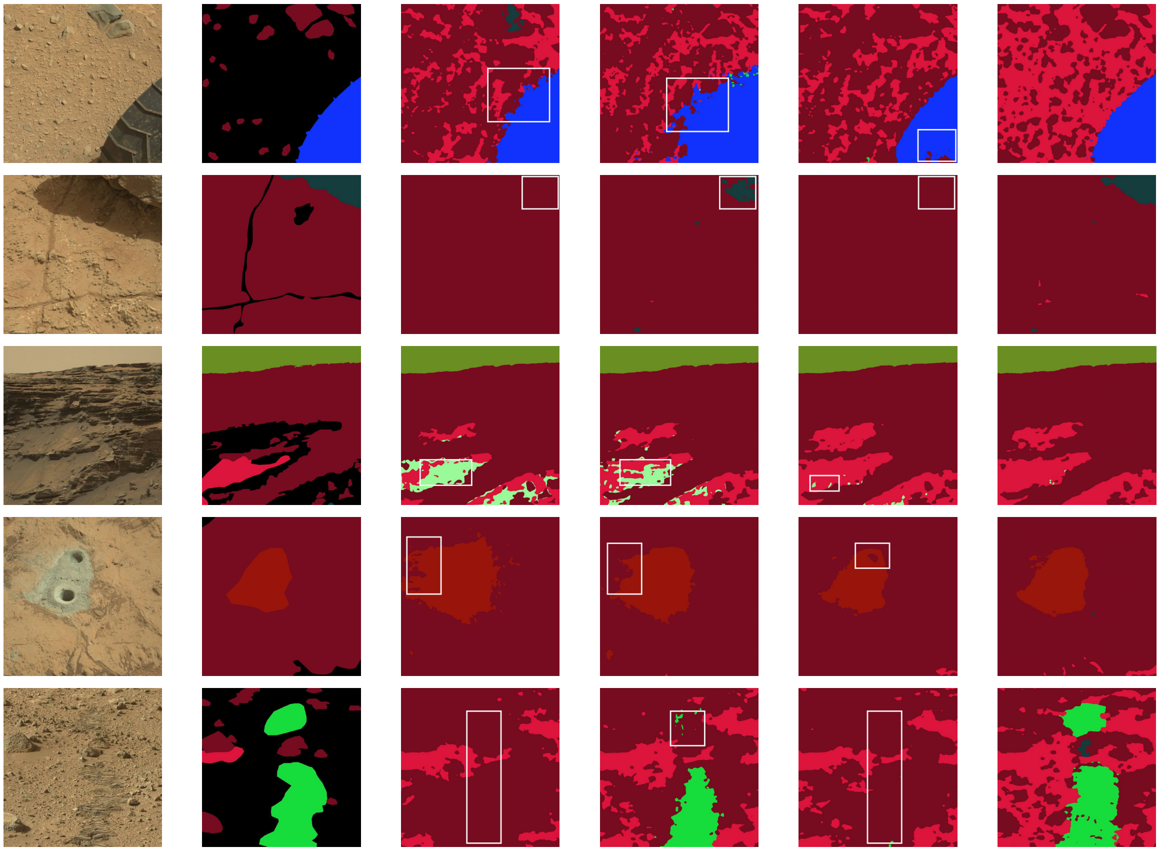

Fig. 10. Qualitative results on S^{5}Mars dataset with full labels. Columns from left to right denote the original images, the ground truth, the supervised results, the MT [47] + ClassMix [50] results, AugSeg [11] results, and our method results, respectively.

4) Confidence-Based Thresholding Strategy: We utilize hard pseudolabels in highly confident regions ($>t_{\text{hard}}$) while using soft labels in regions with low confidence ($<t_{\text{soft}}$). Table XI gives the results of different thresholds. For the hard labels, a too-high threshold (>0.7) can significantly reduce the number of training labels, limiting the effect of pseudolabels. Meanwhile, a too-low threshold can degrade the performance slightly due to the additional introduced uncertain pseudolabels in model consistency learning. However, this effect is relatively weak because only few pixels are involved. For the soft labels, we discard the high confidence region because these regions can be considered reliable and the model should give predictions with high confidence. In this case, correlations generated with other semantic prototypes are often noise, which is not conducive to consistency learning, as shown in Table XII. However, a too-low threshold degrades the performance significantly, which is because these learning targets with high uncertainty lead to an unstable learning process.

5) Loss Weight: We further conduct the ablation studies on the loss weight λ_s of the soft pseudolabels $\mathcal{L}_{\text{unsup}}^{\text{soft}}$ in Fig. 9(b). As we can see, the model performance degrades when the loss weight is too large. This indicates the hard pseudolabel signals of the high-confidence regions are important to the model, which constrains the model predictions to be with low entropy. For the loss weight λ_{unsup}, we set it to be 2.0 following the previous works [10], [11] to make our method more general.

TABLE XIII
COMPLEXITY ANALYSIS ON THE S^{5}MARS DATASET

Methods	Training Time	Params	mIoU (%)
U^{2}PL [38]	98.7h	196.15M	78.60
FixMatch [10]	34.3h	40.47M	73.69
AugSeg [11]	35.9h	80.94M	76.90
Ours	42.8h	80.94M	**80.15**

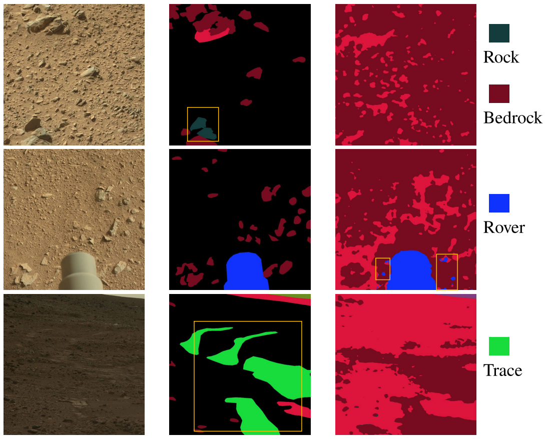

Fig. 11. Some failure cases of our method. From (left) to (right) are the original image, the ground-truth label, and the predicted result.

6) Complexity Analysis: We first present the results of U^{2}PL [38] based on contrastive learning in Table XIII. These methods have high complexity because they need to maintain a large number of samples in the memory bank and perform instance discrimination tasks with multiple negative samples. As we can see, our method based on consistency regularization has an obvious complexity advantage, which shows the advantage of this type of method for extraterrestrial missions. Compared with other consistency-regularization methods [10], [11], our method has a longer training time due to the additional back-propagation process for soft pseudolabel optimization and data augmentations. Since the same backbone network is used, the inference time is the same across these methods. As for the model parameters, the difference lies in whether the teacher and student models share parameters. Despite the cost incurred in terms of training time and space parameters, we argue that they are acceptable where a significant performance gain is observed.

E. Qualitative Results

We present subjective segmentation results in Fig. 10. The compared methods employ the same ResNet50 backbone. As we can see, the segmentation results of our method are more accurate than other methods, which is reflected in clearer object contours (first and fourth rows), more sensitive and accurate object detection (second and fifth rows), and less category mixing in segmentation map (third row). Compared with AugSeg [11] that is also based on two-branch architecture but with many color augmentations, our method can generate better results, demonstrating the effectiveness of the proposed augmentations for the SSL Mars segmentation task.

F. Limitations and Discussions

Our method is efficiently designed in terms of data augmentation and pseudolabel optimization for the semi-supervised Mars segmentation task. Notably, it scales well with the existing techniques, e.g., augmentation anchoring and distribution alignment in [67], and is simple to implement, making it a strong model to provide the basis for future work.

We present some failure cases in Fig. 11 As we can see, the limitations mainly lie in two aspects.

1) There is confusion between similar categories as shown in the first case. For example, to distinguish the rock and bedrock, the model needs to classify whether the rock is exposed to the ground, which can be difficult. One direction is to carry out specific designs, e.g., training an independent classifier, for these difficult categories.
2) The images directly taken by the rovers on Mars often have a long-tailed label distribution, which may affect the reliability of the pseudolabels in SSL, causing the noisy prediction or misclassification in the tail classes as shown in the second and third cases. We point out these observed problems as future work, in the hope that more meaningful works will emerge.

VI. Conclusion

In this article, we address the SSL for Mars semantic segmentation problem from both data and method perspectives. First, we propose a fine-grained annotated dataset S^{5}Mars for Martian terrain segmentation. This dataset provides sparse and high-confidence labeled data, which effectively assists the subsequent Mars exploration work. Then, we propose a simple yet effective SSL framework. Specifically, we analyze the effect of currently used augmentations for Mars image segmentation. Two effective augmentations, AugIN and SAM-Mix, are further proposed to improve the model performance. Meanwhile, a soft-to-hard consistency learning strategy is introduced to fully utilize the unlabeled data in a confidence-based manner. Extensive comparison and ablation experiments demonstrate the effectiveness of our method.

References

[1] D. Qiu et al., “SCOTI: Science captioning of terrain images for data prioritization and local image search,” *Planet. Space Sci.*, vol. 188, Sep. 2020, Art. no. 104943.

[2] F. Goesmann et al., “The Mars organic molecule analyzer (MOMA) instrument: Characterization of organic material in Martian sediments,” *Astrobiology*, vol. 17, nos. 6–7, pp. 655–685, Jul. 2017.

[3] V. DaPoian, E. Lyness, W. Brinckerhoff, R. Danell, X. Li, and M. Trainer, “Science autonomy and the ExoMars mission: Machine learning to help find life on Mars,” *Computer*, vol. 54, no. 10, pp. 69–77, Oct. 2021.

[4] I. Priyadarshini and V. Puri, “Mars weather data analysis using machine learning techniques,” *Earth Sci. Informat.*, vol. 14, no. 4, pp. 1885–1898, Dec. 2021.

[5] R. Gonzalez and K. Iagnemma, “DeepTerramechanics: Terrain classification and slip estimation for ground robots via deep learning,” 2018, *arXiv:1806.07379*.

[6] M. Dimastrogiovanni, F. Cordes, and G. Reina, “Terrain estimation for planetary exploration robots,” *Appl. Sci.*, vol. 10, no. 17, p. 6044, Aug. 2020.

[7] S. P. Schwenzer, M. Woods, S. Karachalios, N. Phan, and L. Joudrier, “LabelMars: Clesting an extremely large martian image dataset through machine learning,” in *Proc. Lunar Planet. Sci. Conf.*, 2019, p. 1970.

[8] R. M. Swan et al., “AI4MARS: A dataset for terrain-aware autonomous driving on Mars,” in *Proc. IEEE/CVF Conf. Comput. Vis. Pattern Recognit. Workshops (CVPRW)*, Jun. 2021, pp. 1982–1991.

[9] B. Rothrock, R. Kennedy, C. Cunningham, J. Papon, M. Heverly, and M. Ono, “SPOC: Deep learning-based terrain classification for Mars rover missions,” in *Proc. AIAA SPACE*, 2016, p. 5539.

[10] K. Sohn et al., “FixMatch: Simplifying semi-supervised learning with consistency and confidence,” in *Proc. NIPS*, 2020, pp. 596–608.

[11] Z. Zhao, L. Yang, S. Long, J. Pi, L. Zhou, and J. Wang, “Augmentation matters: A simple-yet-effective approach to semi-supervised semantic segmentation,” in *Proc. CVPR*, 2023, pp. 11350–11359.

[12] L. Yang, L. Qi, L. Feng, W. Zhang, and Y. Shi, “Revisiting weak-to-strong consistency in semi-supervised semantic segmentation,” in *Proc. CVPR*, 2023, pp. 7236–7246.

[13] J. Yuan, Y. Liu, C. Shen, Z. Wang, and H. Li, “A simple baseline for semi-supervised semantic segmentation with strong data augmentation,” in *Proc. IEEE/CVF Int. Conf. Comput. Vis. (ICCV)*, Oct. 2021, pp. 8209–8218.

[14] A. Kirillov et al., “Segment anything,” 2023, *arXiv:2304.02643*.

[15] J. Li et al., “Autonomous Martian rock image classification based on transfer deep learning methods,” *Earth Sci. Informat.*, vol. 13, no. 3, pp. 951–963, Sep. 2020.

[16] K. Wagstaff, Y. Lu, A. Stanboli, K. Grimes, T. Gowda, and J. Padams, “Deep Mars: CNN classification of Mars imagery for the PDS imaging atlas,” in *Proc. AAAI*, 2018, pp. 7867–7872.

[17] X. Xiao, M. Yao, H. Liu, J. Wang, L. Zhang, and Y. Fu, “A kernel-based multi-featured rock modeling and detection framework for a Mars rover,” *IEEE Trans. Neural Netw. Learn. Syst.*, vol. 34, no. 7, pp. 3335–3344, Jul. 2023.

[18] H. Liu, M. Yao, X. Xiao, and Y. Xiong, “RockFormer: A U-shaped transformer network for Martian rock segmentation,” *IEEE Trans. Geosci. Remote Sens.*, vol. 61, pp. 1–16, 2023, doi: 10.1109/TGRS.2023.3235525.

[19] H. R. Kerner, J. F. Bell, and H. Ben Amor, "Context-dependent image quality assessment of JPEG compressed Mars science laboratory mastcam images using convolutional neural networks," *Comput. Geosci.*, vol. 118, pp. 109–121, Sep. 2018.

[20] D. R. Thompson and R. Castano, "Performance comparison of rock detection algorithms for autonomous planetary geology," in *Proc. IEEE Aerosp. Conf.*, Mar. 2007, pp. 1–9.

[21] D. R. Thompson et al., "Smart cameras for remote science survey," in *Proc. Int. Symp. Artif. Intell. Robot. Automat. Space*. Pasadena, CA, USA: Jet Propulsion Laboratory, National Aeronautics and Space, 2012.

[22] J. Li, S. Zi, R. Song, Y. Li, Y. Hu, and Q. Du, "A stepwise domain adaptive segmentation network with covariate shift alleviation for remote sensing imagery," *IEEE Trans. Geosci. Remote Sens.*, vol. 60, pp. 1–15, 2022.

[23] T. Wilhelm et al., "DoMars16k: A diverse dataset for weakly supervised geomorphologic analysis on Mars," *Remote Sens.*, vol. 12, no. 23, p. 3981, Dec. 2020.

[24] S. Niekum, "Reliable rock detection and classification for autonomous science," Ph.D. thesis, Carnegie Mellon Univ., Pittsburgh, PA, USA, Jun. 2005. [Online]. Available: https://people.cs.umass.edu/~sniekum/pubs/SeniorThesis.pdf

[25] S. Higa et al., "Vision-based estimation of driving energy for planetary rovers using deep learning and terramechanics," *IEEE Robot. Autom. Lett.*, vol. 4, no. 4, pp. 3876–3883, Oct. 2019.

[26] F. Fán, E. Rubio, H. Sossa, and V. Ponce, "Rock detection in a Mars-like environment using a CNN," in *Proc. Mex. Conf. Pattern Recognit.*, 2019, pp. 149–158.

[27] X. Xiao, H. Cui, M. Yao, and Y. Tian, "Autonomous rock detection on Mars through region contrast," *Adv. Space Res.*, vol. 60, no. 3, pp. 626–635, Aug. 2017.

[28] L.-C. Chen, Y. Zhu, G. Papandreou, F. Schroff, and H. Adam, "Encoder–decoder with atrous separable convolution for semantic image segmentation," in *Proc. ECCV*, 2018, pp. 801–818.

[29] E. Goh, J. Chen, and B. Wilson, "Mars terrain segmentation with less labels," 2022, *arXiv:2202.00791*.

[30] Y. Xiong, X. Xiao, M. Yao, H. Liu, H. Yang, and Y. Fu, "MarsFormer: Martian rock semantic segmentation with transformer," *IEEE Trans. Geosci. Remote Sens.*, vol. 61, pp. 1–12, 2023.

[31] J. Zhang, Y. Xia, and G. Shen, "A novel deep neural network architecture for mars visual navigation," 2018, *arXiv:1808.08395*.

[32] M. Ono et al., "MAARS: Machine learning-based analytics for automated rover systems," in *Proc. IEEE Aerosp. Conf.*, Mar. 2020, pp. 1–17.

[33] C. Liu et al., "Progressive neural architecture search," in *Proc. ECCV*, 2018, pp. 19–34.

[34] B. Sun and K. Saenko, "Deep coral: Correlation alignment for deep domain adaptation," in *Proc. ECCVW*, 2016, pp. 443–450.

[35] J. Lambert, Z. Liu, O. Sener, J. Hays, and V. Koltun, "MSeg: A composite dataset for multi-domain semantic segmentation," in *Proc. IEEE/CVF Conf. Comput. Vis. Pattern Recognit. (CVPR)*, Jun. 2020, pp. 2876–2885.

[36] Y. Ouali, C. Hudelot, and M. Tami, "An overview of deep semi-supervised learning," 2020, *arXiv:2006.05278*.

[37] Q. Xie, M.-T. Luong, E. Hovy, and Q. V. Le, "Self-training with noisy student improves ImageNet classification," in *Proc. IEEE/CVF Conf. Comput. Vis. Pattern Recognit. (CVPR)*, Jun. 2020, pp. 10684–10695.

[38] Y. Wang et al., "Semi-supervised semantic segmentation using unreliable pseudo-labels," in *Proc. IEEE/CVF Conf. Comput. Vis. Pattern Recognit. (CVPR)*, Jun. 2022, pp. 4238–4247.

[39] Y. Zhong, B. Yuan, H. Wu, Z. Yuan, J. Peng, and Y.-X. Wang, "Pixel contrastive-consistent semi-supervised semantic segmentation," in *Proc. IEEE/CVF Int. Conf. Comput. Vis. (ICCV)*, Oct. 2021, pp. 7253–7262.

[40] L. Hu et al., "Semi-supervised NPC segmentation with uncertainty and attention guided consistency," *Knowl.-Based Syst.*, vol. 239, Mar. 2022, Art. no. 108021.

[41] R. Mendel, L. A. De Souza, D. Rauber, J. P. Papa, and C. Palm, "Semi-supervised segmentation based on error-correcting supervision," in *Proc. ECCV*, 2020, pp. 141–157.

[42] D. Berthelot, N. Carlini, I. Goodfellow, N. Papernot, A. Oliver, and C. A. Raffel, "MixMatch: A holistic approach to semi-supervised learning," in *Proc. NIPS*, 2019, pp. 5049–5059.

[43] H. Zhang, M. Cisse, Y. N. Dauphin, and D. Lopez-Paz, "mixup: Beyond empirical risk minimization," 2017, *arXiv:1710.09412*.

[44] B. Zhang et al., "FlexMatch: Boosting semi-supervised learning with curriculum pseudo labeling," in *Proc. NIPS*, 2021, pp. 18408–18419.

[45] Y. Wang et al., "FreeMatch: Self-adaptive thresholding for semi-supervised learning," 2022, *arXiv:2205.07246*.

[46] E. D. Cubuk, B. Zoph, J. Shlens, and Q. V. Le, "Randaugment: Practical automated data augmentation with a reduced search space," in *Proc. IEEE/CVF Conf. Comput. Vis. Pattern Recognit. Workshops (CVPRW)*, Jun. 2020, pp. 3008–3017.

[47] A. Tarvainen and H. Valpola, "Mean teachers are better role models: Weight-averaged consistency targets improve semi-supervised deep learning results," in *Proc. NIPS*, 2017, pp. 1195–1204.

[48] S. Yun, D. Han, S. Chun, S. J. Oh, Y. Yoo, and J. Choe, "CutMix: Regularization strategy to train strong classifiers with localizable features," in *Proc. ICCV*, 2019, pp. 6023–6032.

[49] G. French, A. Oliver, and T. Salimans, "Milking CowMask for semi-supervised image classification," 2020, *arXiv:2003.12022*.

[50] V. Olsson, W. Tranheden, J. Pinto, and L. Svensson, "ClassMix: Segmentation-based data augmentation for semi-supervised learning," in *Proc. IEEE Winter Conf. Appl. Comput. Vis. (WACV)*, Jan. 2021, pp. 1368–1377.

[51] N. Srivastava, G. Hinton, A. Krizhevsky, I. Sutskever, and R. Salakhutdinov, "Dropout: A simple way to prevent neural networks from overfitting," *J. Mach. Learn. Res.*, vol. 15, no. 1, pp. 1929–1958, 2014.

[52] J. Deng, W. Dong, R. Socher, L.-J. Li, K. Li, and L. Fei-Fei, "ImageNet: A large-scale hierarchical image database," in *Proc. IEEE Conf. Comput. Vis. Pattern Recognit.*, Jun. 2009, pp. 248–255.

[53] X. Huang and S. Belongie, "Arbitrary style transfer in real-time with adaptive instance normalization," in *Proc. IEEE Int. Conf. Comput. Vis. (ICCV)*, Oct. 2017, pp. 1510–1519.

[54] G. French, S. Laine, T. Aila, M. Mackiewicz, and G. Finlayson, "Semi-supervised semantic segmentation needs strong, varied perturbations," 2019, *arXiv:1906.01916*.

[55] D. Dwibedi, I. Misra, and M. Hebert, "Cut, paste and learn: Surprisingly easy synthesis for instance detection," in *Proc. IEEE Int. Conf. Comput. Vis. (ICCV)*, Oct. 2017, pp. 1310–1319.

[56] S. Tripathi, S. Chandra, A. Agrawal, A. Tyagi, J. M. Rehg, and V. Chari, "Learning to generate synthetic data via compositing," in *Proc. IEEE/CVF Conf. Comput. Vis. Pattern Recognit. (CVPR)*, Jun. 2019, pp. 461–470.

[57] H.-S. Fang, J. Sun, R. Wang, M. Gou, Y.-L. Li, and C. Lu, "InstaBoost: Boosting instance segmentation via probability map guided copy-pasting," in *Proc. Int. Conf. Comput. Vis.*, Oct. 2019, pp. 682–691.

[58] Y. Yang and S. Soatto, "FDA: Fourier domain adaptation for semantic segmentation," in *Proc. IEEE/CVF Conf. Comput. Vis. Pattern Recognit. (CVPR)*, Jun. 2020, pp. 4084–4094.

[59] W. Park, D. Kim, Y. Lu, and M. Cho, "Relational knowledge distillation," in *Proc. IEEE/CVF Conf. Comput. Vis. Pattern Recognit. (CVPR)*, Jun. 2019, pp. 3962–3971.

[60] K. He, X. Zhang, S. Ren, and J. Sun, "Deep residual learning for image recognition," in *Proc. IEEE Conf. Comput. Vis. Pattern Recognit. (CVPR)*, Jun. 2016, pp. 770–778.

[61] J.-X. Wang, S.-B. Chen, C. H. Q. Ding, J. Tang, and B. Luo, "RanPaste: Paste consistency and pseudo label for semisupervised remote sensing image semantic segmentation," *IEEE Trans. Geosci. Remote Sens.*, vol. 60, pp. 1–16, 2021.

[62] M. Xu, Z. Zhang, F. Wei, H. Hu, and X. Bai, "Side adapter network for open-vocabulary semantic segmentation," in *Proc. CVPR*, 2023, pp. 2945–2954.

[63] A. Radford et al., "Learning transferable visual models from natural language supervision," in *Proc. ICML*, 2021, pp. 8748–8763.

[64] Y. Zhang, M. Li, R. Li, K. Jia, and L. Zhang, "Exact feature distribution matching for arbitrary style transfer and domain generalization," in *Proc. IEEE/CVF Conf. Comput. Vis. Pattern Recognit. (CVPR)*, Jun. 2022, pp. 8025–8035.

[65] Y. Li, C. Fang, J. Yang, Z. Wang, X. Lu, and M.-H. Yang, "Universal style transfer via feature transforms," in *Proc. NIPS*, 2017, pp. 385–395.

[66] W. Tranheden, V. Olsson, J. Pinto, and L. Svensson, "DACS: Domain adaptation via cross-domain mixed sampling," in *Proc. IEEE Winter Conf. Appl. Comput. Vis. (WACV)*, Jan. 2021, pp. 1378–1388.

[67] D. Berthelot et al., "ReMixMatch: Semi-supervised learning with distribution alignment and augmentation anchoring," 2019, *arXiv:1911.09785*.

Jiahang Zhang received the B.S. degree in computer science from Peking University, Beijing, China, in 2023, where he is currently pursuing the Ph.D. degree with the Wangxuan Institute of Computer Technology.

His research interests include action recognition and self-supervised learning.

Lilang Lin (Student Member, IEEE) received the B.S. degree in data science from Peking University, Beijing, China, in 2021, where he is currently pursuing the Ph.D. degree with the Wangxuan Institute of Computer Technology.

His research interests include action recognition, self-supervised learning, and unsupervised learning.

Zejia Fan received the B.S. degree in computer science from Peking University, Beijing, China, in 2021, where she is currently pursuing the Ph.D. degree with the Wangxuan Institute of Computer Technology.

Her research interests include image enhancement and deep learning.

Wenjing Wang (Graduate Student Member, IEEE) received the B.S. degree in data science from Peking University, Beijing, China, in 2019, where she is currently pursuing the Doctoral degree with the Wangxuan Institute of Computer Technology.

She has authored over 20 technical articles in refereed journals and proceedings, and she holds five granted patents. Her research interests include image enhancement, image synthesis, and deep learning.

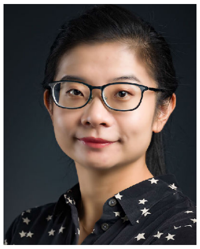

Jiaying Liu (Senior Member, IEEE) received the Ph.D. degree (Hons.) in computer science from Peking University, Beijing China, 2010.

She was a Visiting Scholar with the University of Southern California, Los Angeles, CA, USA, from 2007 to 2008. She was a Visiting Researcher with Microsoft Research Asia, Beijing, in 2015 supported by the Star Track Young Faculties Award. She is currently an Associate Professor and a Boya Young Fellow with the Wangxuan Institute of Computer Technology, Peking University. She has authored more than 100 technical articles in refereed journals and proceedings, and holds 70 granted patents. Her research interests include multimedia signal processing, compression, and computer vision.

Dr. Liu is a Senior Member of CSIG and a Distinguished Member of CCF. She has served as a member of the Multimedia Systems and Applications Technical Committee (MSA TC) and the Visual Signal Processing and Communications Technical Committee (VSPC TC) in the IEEE Circuits and Systems Society. She received the IEEE ICME 2020 Best Paper Award and IEEE MMSP 2015 Top10% Paper Award. She was the Technical Program Chair of ACM MM Asia-2023/IEEE ICME-2021/ACM ICMR-2021/IEEE VCIP-2019, the Area Chair of CVPR-2021/ECCV-2020/ICCV-2019, the ACM ICMR Steering Committee Member, and the CAS Representative at the ICME Steering Committee. She was the APSIPA Distinguished Lecturer from 2016 to 2017. She has served as an Associate Editor of IEEE TRANSACTIONS ON IMAGE PROCESSING, IEEE TRANSACTIONS ON CIRCUITS SYSTEMS FOR VIDEO TECHNOLOGY, and *Journal of Visual Communication and Image Representation*.